Deterministic All-Optical Continuous-Variable Quantum Telecloning

Yanbo Lou,[1,*] Yinghui Lv,[1,*] Jiabin Wang,[1] Shengshuai Liu,[1,†] and Jietai Jing[1,2,3,‡]
[1]State Key Laboratory of Precision Spectroscopy, Joint Institute of Advanced Science and Technology, School of Physics and Electronic Science, East China Normal University, Shanghai 200062, China
[2]CAS Center for Excellence in Ultra-intense Laser Science, Shanghai 201800, China
[3]Collaborative Innovation Center of Extreme Optics, Shanxi University, Taiyuan, Shanxi 030006, China

(Received 13 July 2023; accepted 25 March 2024; published 18 April 2024)

Quantum telecloning, a pivotal multiuser quantum communication protocol in the realm of quantum information science, facilitates the copy of a quantum state across M distinct locations through teleportation technique. In the continuous-variable regime, the implementation of quantum telecloning necessitates the distribution of multipartite entanglement among the sender and M receiver parties. Following this, the sender carries out optic-electro conversion and transmits information via classical channel to M spatially separated receivers simultaneously. To successfully reconstruct the input state, electro-optic conversion needs to be employed by each receiver. However, due to these conversions, the bandwidth of the optical mode in this process is largely constrained. In this Letter, we present an all-optical version of the $1 \rightarrow 2$ continuous-variable quantum telecloning scheme, wherein both optic-electro and electro-optic conversions are replaced by optical components. Our scheme allows the two receivers to achieve input state reconstruction solely by utilizing beam splitters, significantly simplifying its complexity. We experimentally demonstrate all-optical $1 \rightarrow 2$ quantum telecloning of coherent state and achieve the fidelities of $58.6\% \pm 1.0\%$ and $58.6\% \pm 1.1\%$ for two clones, exceeding the corresponding classical limits ($51.9\% \pm 0.5\%$ and $51.9\% \pm 0.6\%$). Our results establish a platform for constructing a flexible all-optical multiuser quantum network and promote the field of all-optical quantum information processing.

DOI: 10.1103/PhysRevLett.132.160803

The no-cloning theorem [1,2] in quantum physics holds that it is impossible to perfectly clone or copy an unknown quantum state. Nevertheless, the approximation cloning of quantum state with a nonunit fidelity is feasible, leading to the investigation of quantum cloning machines for achieving optimal "local" quantum state cloning [3–5]. In the continuous-variable (CV) regime, the quantum cloning machine has been studied in both theory [6–9] and experiment [10–13]. Quantum teleportation [14–22], which transfers an unknown quantum state from one location to another with the help of quantum entanglement, is a nonlocal quantum information protocol. Different from quantum cloning and quantum teleportation protocol, quantum telecloning [23,24], which can achieve optimal quantum state cloning at multiple nonlocal locations by integrating quantum teleportation and quantum cloning into a unified quantum information protocol, is one of the most important multiuser quantum information protocols. Compared to the conventional two-step scheme of initially performing local optimal quantum cloning [4,5] and then conducting quantum teleportation on individual clones, the requirement of the quantum telecloning protocol for entanglement resources is relatively relaxed. For CV coherent state nonlocal cloning, the two-step scheme requires infinite entanglement resources for achieving optimal cloning fidelity, while the quantum telecloning protocol requires only finite entanglement resources. CV coherent state $1 \rightarrow 2$ and $1 \rightarrow 3$ quantum telecloning protocols have been demonstrated experimentally [25,26]. The implementation of such a protocol facilitates the development of CV multiuser quantum information and quantum communication and makes it possible to distribute a quantum state with high fidelity in the CV quantum network.

In the CV regime, conventional quantum teleportation technology [14–17] achieves quantum state transmission by utilizing a feed-forward technique encompassing optic-electro and electro-optic conversions. Therefore, the bandwidth of the optical mode in this process is largely constrained [27]. Moreover, for implementing quantum telecloning by such a feed-forward technique, each receiver needs to implement displacement operation through amplitude and phase modulators. These constraints hinder the flexibility and conciseness of implementing the CV quantum telecloning protocol.

Unlike the standard quantum teleportation protocol, quantum state transfer can be achieved by an all-optical version [18–20], wherein the optic-electro and electro-optic conversions are replaced by optical devices. This all-optical scheme provides a solution for the concise reconstruction of information and makes the transmission of information without the bandwidth constraints. Therefore, it is important to develop an all-optical version of quantum telecloning based on such an all-optical scheme. In this Letter, we experimentally demonstrate an all-optical version of the CV quantum telecloning protocol by integrating the all-optical quantum teleportation and quantum cloning

 © 2024 American Physical Society

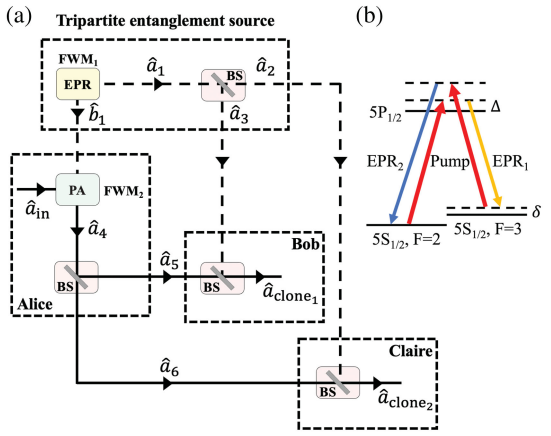

FIG. 1. Schematic of all-optical $1 \rightarrow 2$ CV quantum telecloning. (a) The scheme of all-optical $1 \rightarrow 2$ quantum telecloning protocol. EPR, Einstein-Podolsky-Rosen entangled source; PA, parametric amplifier; FWM, four-wave mixing; BS, beam splitter; $\hat{a}_1$ and $\hat{b}_1$, the annihilation operators associated with beams EPR_1 and EPR_2, respectively; $\hat{a}_{\mathrm{in}}$, the annihilation operator associated with input state; $\hat{a}_4$, the annihilation operator associated with amplified $\hat{a}_{\mathrm{in}}$; $\hat{a}_{\mathrm{clone}_1}$ ($\hat{a}_{\mathrm{clone}_2}$), the annihilation operator associated with the clone state; Alice, sender; Bob and Claire, receivers. (b) Energy level structure of the double-Λ FWM process in the $D1$ line of ^{85}Rb. Δ, one-photon detuning; δ, two-photon detuning.

protocols. In such a protocol, a phase-insensitive amplifier based on a double-Λ configuration four-wave mixing (FWM) process [28–33] is utilized to replace the joint quadrature measurement, and each receiver at different locations can achieve quantum cloning of the initial quantum state solely through an optical beam splitter (BS) [9]. We experimentally realize all-optical coherent state $1 \rightarrow 2$ CV quantum telecloning with fidelities of $58.6\% \pm 1.0\%$ and $58.6\% \pm 1.1\%$ for two clones, which surpass the classical limit.

The scheme for all-optical $1 \rightarrow 2$ CV quantum telecloning protocol is shown in Fig. 1(a). To achieve all-optical $1 \rightarrow 2$ quantum telecloning, it is necessary to generate tripartite entanglement comprised of both bipartite and tripartite structure [25] and distribute tripartite entanglement among the sender and two receivers. In our scheme, we first generate the Einstein-Podolsky-Rosen (EPR) entanglement state [34–36] from the double-Λ configuration FWM process in ^{85}Rb vapor cell (FWM_1). The energy level structure of such a FWM process is shown in Fig. 1(b). In this process, two pump photons convert to one photon of the probe beam (redshifted from the pump beam) and one photon of the conjugate beam (blueshifted from the pump beam). Therefore, the interaction Hamiltonian of FWM_1 can be expressed as

$$\hat{H}_1 = i\hbar\gamma_1 \hat{a}_1^{\dagger}\hat{b}_1^{\dagger} + \mathrm{H.c.}, \tag{1}$$

where $\hat{a}_1^{\dagger}$ and $\hat{b}_1^{\dagger}$ are the creation operators associated with the EPR_1 (probe beam) and EPR_2 (conjugate beam) for FWM_1, respectively. H.c. is the Hermitian conjugate. γ_1 denotes the interaction strength of FWM_1. Based on Eq. (1), the input-output relation of FWM_1 can be expressed as

$$\begin{aligned} \hat{a}_1 &= \sqrt{G_1}\hat{v}_1 + \sqrt{G_1 - 1}\hat{v}_2^{\dagger}, \\ \hat{b}_1^{\dagger} &= \sqrt{G_1 - 1}\hat{v}_1 + \sqrt{G_1}\hat{v}_2^{\dagger}, \end{aligned} \tag{2}$$

where $\hat{v}_1$ and $\hat{v}_2$ are the annihilation operators of the vacuum states introduced by FWM_1. $G_1 = \cosh^2(\gamma_1\tau)$ is the intensity gain of the FWM_1, and τ is the interaction time. Then, one beam of the EPR entanglement state $\hat{a}_1$ is divided into two by a BS with a transmittance of $1/2$, i.e., the beams $\hat{a}_2 = (\hat{a}_1 + \hat{v}_3)/\sqrt{2}$ and $\hat{a}_3 = (\hat{a}_1 - \hat{v}_3)/\sqrt{2}$. $\hat{v}_3$ is the vacuum state introduced by BS. The beams $\hat{b}_1$, $\hat{a}_2$, and $\hat{a}_3$ form a tripartite entanglement source [25,37]. Moreover, the beams $\hat{b}_1$ and $\hat{a}_2$ ($\hat{b}_1$ and $\hat{a}_3$) are bipartite entanglement [38], which allows the sender Alice to simultaneously implement quantum teleportation among two receivers Bob and Claire. The sender Alice performs an all-optical operation by amplifying the input state $\hat{a}_{\mathrm{in}}$ and $\hat{b}_1$ with a parametric amplifier (PA) based on the other FWM process (FWM_2). Therefore, the amplified input state $\hat{a}_4$ can be expressed as

$$\hat{a}_4 = \sqrt{G_2}\hat{a}_{\mathrm{in}} + \sqrt{G_2 - 1}\hat{b}_1^{\dagger}, \tag{3}$$

where $\hat{a}_{\mathrm{in}}$ is the annihilation operator of the input coherent state. $G_2 = \cosh^2(\gamma_2\tau)$ is the intensity gain of the PA. γ_2 denotes the interaction strength of FWM_2. The beam $\hat{a}_4$ is also divided into two beams $\hat{a}_5 = (\hat{a}_4 + \hat{v}_4)/\sqrt{2}$ and $\hat{a}_6 = (\hat{a}_4 - \hat{v}_4)/\sqrt{2}$ by a BS with a transmittance of $1/2$. $\hat{v}_4$ is the vacuum state introduced by BS. The beams $\hat{a}_5$ and $\hat{a}_6$ are distributed to Bob and Claire, respectively, through all-optical classical channels. Then, Bob couples the beams $\hat{a}_3$ and $\hat{a}_5$ by BS with a transmittance of $\varepsilon_1 = 2/G_2$, and Claire also couples the beams $\hat{a}_2$ and $\hat{a}_6$ by BS with the same transmittance of $\varepsilon_2 = 2/G_2$. Therefore, the two clone states reconstructed by Bob and Claire can be described as

$$\begin{aligned} \hat{a}_{\mathrm{clone}_1} = \hat{a}_{\mathrm{in}} &+ \left[\sqrt{\frac{(G_1-1)(G_2-1)}{G_2}} - \sqrt{\frac{G_1(G_2-2)}{2G_2}}\right]\hat{v}_1 \\ &+ \left[\sqrt{\frac{G_1(G_2-1)}{G_2}} - \sqrt{\frac{(G_1-1)(G_2-2)}{2G_2}}\right]\hat{v}_2^{\dagger} \\ &+ \sqrt{\frac{G_2-2}{2G_2}}\hat{v}_3 + \frac{1}{\sqrt{G_2}}\hat{v}_4, \\ \hat{a}_{\mathrm{clone}_2} = \hat{a}_{\mathrm{in}} &+ \left[\sqrt{\frac{(G_1-1)(G_2-1)}{G_2}} - \sqrt{\frac{G_1(G_2-2)}{2G_2}}\right]\hat{v}_1 \\ &+ \left[\sqrt{\frac{G_1(G_2-1)}{G_2}} - \sqrt{\frac{(G_1-1)(G_2-2)}{2G_2}}\right]\hat{v}_2^{\dagger} \\ &- \sqrt{\frac{G_2-2}{2G_2}}\hat{v}_3 - \frac{1}{\sqrt{G_2}}\hat{v}_4. \end{aligned} \tag{4}$$

When $G_1 = 2$ and $G_2 \gg 1$, the two clone states can be reduced as

$$\hat{a}_{\text{clone}_1} \approx \hat{a}_{\text{in}} + \frac{1}{\sqrt{2}}\hat{v}_2^{\dagger} + \frac{1}{\sqrt{2}}\hat{v}_3,$$
$$\hat{a}_{\text{clone}_2} \approx \hat{a}_{\text{in}} + \frac{1}{\sqrt{2}}\hat{v}_2^{\dagger} - \frac{1}{\sqrt{2}}\hat{v}_3. \tag{5}$$

The performance of telecloning can be characterized by the overlap between the input coherent state and the clone, i.e., the fidelity. The fidelity of all-optical $1 \to 2$ quantum telecloning protocol can be expressed as [39]

$$F = 2/\sqrt{(1+\Delta^2\hat{X}_{\text{clone}_i})(1+\Delta^2\hat{Y}_{\text{clone}_i})}, \tag{6}$$

where $\hat{X}_{\text{clone}_i} = (\hat{a}_{\text{clone}_i} + \hat{a}^{\dagger}_{\text{clone}_i})$ and $\hat{Y}_{\text{clone}_i} = i(\hat{a}^{\dagger}_{\text{clone}_i} - \hat{a}_{\text{clone}_i})$ are the amplitude and phase quadratures of the clone $\hat{a}_{\text{clone}_i}$ for $i = 1, 2$, respectively. $\Delta^2\hat{X}_{\text{clone}_i}$ and $\Delta^2\hat{Y}_{\text{clone}_i}$ are defined as the fluctuation variances. If the fidelity F_{clone_i} exceeds the classical limits $F_{\text{classical}}$ obtained by blocking the tripartite entanglement, our all-optical $1 \to 2$ quantum telecloning protocol will be successful. Based on Eqs. (5) and (6), in the ideal case, we can find $\Delta^2\hat{X}_{\text{clone}_i} = \Delta^2\hat{Y}_{\text{clone}_i} = 2$ and $F_{\text{clone}_i} = \frac{2}{3}$, which is equal to the fidelity of the local optimal coherent state $1 \to 2$ quantum cloning [6,11]. It clearly shows that our all-optical quantum telecloning protocol can realize optimal quantum cloning by using finite entanglement resources $(G_1 = 2)$.

The experimental details of all-optical $1 \to 2$ CV quantum telecloning are shown in Fig. 2. The quantum telecloning system starts from a cavity stabilized Ti:sapphire laser whose frequency is about 1 GHz blue detuned from the $D1$ line of ^{85}Rb $(5S_{1/2}, F = 2 \to 5P_{1/2})$. The laser is divided into three parts by two polarization beam splitters (PBSs) and two half-wave plates (HWPs). The first part, injected into a 12-mm-long ^{85}Rb vapor cell with a stable temperature of about 115.5 °C, is used for the pump of the

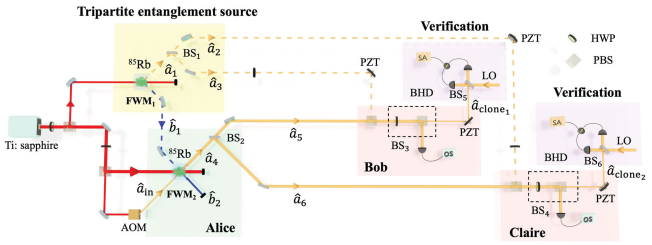

FIG. 2. Detailed experimental setup for all-optical $1 \to 2$ CV quantum telecloning protocol. HWP, half-wave plate; PBS, polarization beam splitter; FWM, four-wave mixing; ^{85}Rb, hot ^{85}Rb vapor cell; BS, beam splitter; AOM, acousto-optic modulator; PZT, piezoelectric transducer; BHD, balanced homodyne detection; LO, local oscillator; OS, oscilloscope; SA, spectrum analyzer. The resolution bandwidth (RBW) of the SA is 1 MHz. The video bandwidth (VBW) of the SA is 100 Hz.

FWM_1 to generate the EPR entanglement state ($\hat{a}_1$ and $\hat{b}_1$). This pump beam, whose waist is about 620 μm at the center of vapor cell, is vertically polarized and has a power of about 50 mW. Then, $\hat{a}_1$ is divided into $\hat{a}_2$ and $\hat{a}_3$ by BS_1 whose transmittance is 1/2, thus forming tripartite entanglement among $\hat{a}_2$, $\hat{a}_3$, and $\hat{b}_1$ [25,37]. The second part passes through an acousto-optic modulator (AOM) to generate the input state $\hat{a}_{\text{in}}$. The input state $\hat{a}_{\text{in}}$, which has a waist of about 280 μm at the center of vapor cell, is horizontally polarized with a power of about 1 μW and red detuned from the pump beam by about 3.04 GHz. The third part, which is vertically polarized and has a power of about 400 mW, is used for the pump of the PA (FWM_2), which is utilized to amplify the input state $\hat{a}_{\text{in}}$ with the assistance of the beam $\hat{b}_1$. The beams $\hat{a}_{\text{in}}$ and $\hat{b}_1$ are symmetrically injected into the other ^{85}Rb vapor cell (about 110 °C) at an angle of 14 mrad, while the pump beam is symmetrically crossed with the beams $\hat{a}_{\text{in}}$ and $\hat{b}_1$ in the same plane. The intensity gain G_2 of PA is set at $10 \gg 1$ to make sure that the amplified input state $\hat{a}_{\text{in}}$ can be regarded as a classical field. After amplifying, the beam $\hat{a}_4$ is equally divided into the beams $\hat{a}_5$ and $\hat{a}_6$ by BS_2, and then the beams $\hat{a}_5$ and $\hat{a}_6$ are distributed to Bob and Claire, respectively, through all-optical channels. We change the relative phase between the beams $\hat{a}_2$ ($\hat{a}_3$) and $\hat{a}_6$ ($\hat{a}_5$) by placing a piezoelectric transducer (PZT) in the optical path of the beam $\hat{a}_2$ ($\hat{a}_3$). To reconstruct the input state, Bob (Claire) couples the beams $\hat{a}_3$ ($\hat{a}_2$) and $\hat{a}_5$ ($\hat{a}_6$) by BS_3 (BS_4), which is composed of HWP and PBS enclosed by a black dashed rectangle. By rotating the HWP, the transmittance of the BS_3 (BS_4) can be set to $2/G_2$, i.e., 1/5. In this way, Bob (Claire) reconstructs the input state solely by utilizing BS, which clearly shows that our all-optical quantum telecloning can largely simplify the complexity of conventional quantum telecloning based on optic-electro and electro-optic conversions. Then, we measure the variances of amplitude and phase quadratures for the two clones $\hat{a}_{\text{clone}_1}$ and $\hat{a}_{\text{clone}_2}$ by balanced homodyne detection (BHD) with a spectrum analyzer (SA), respectively. The relative phase between the beam $\hat{a}_{\text{clone}_1}$ ($\hat{a}_{\text{clone}_2}$) and local oscillator (LO) is changed by a PZT in the optical path of the beam $\hat{a}_{\text{clone}_1}$ ($\hat{a}_{\text{clone}_2}$).

The typical experimental results of our deterministic all-optical coherent state $1 \to 2$ CV quantum telecloning are shown in Fig. 3. In the experiment, we measure the noise power of the two clone states simultaneously. The variances of amplitude and phase quadratures measured at the 1.6 MHz sideband via the BHD of the clone$_1$ (clone$_2$) are shown in Figs. 3(a) and 3(b) [Figs. 3(c) and 3(d)], respectively. The black solid traces are the variances of amplitude quadrature $\hat{X}_{\text{in}}$ and phase quadrature $\hat{Y}_{\text{in}}$ of the input state, as shown in Fig. 3. The blue solid traces shown in Figs. 3(a) and 3(b) [Figs. 3(c) and 3(d)] are the variances of amplitude quadrature $\hat{X}_{\text{clone}_1}$ ($\hat{X}_{\text{clone}_2}$) and phase

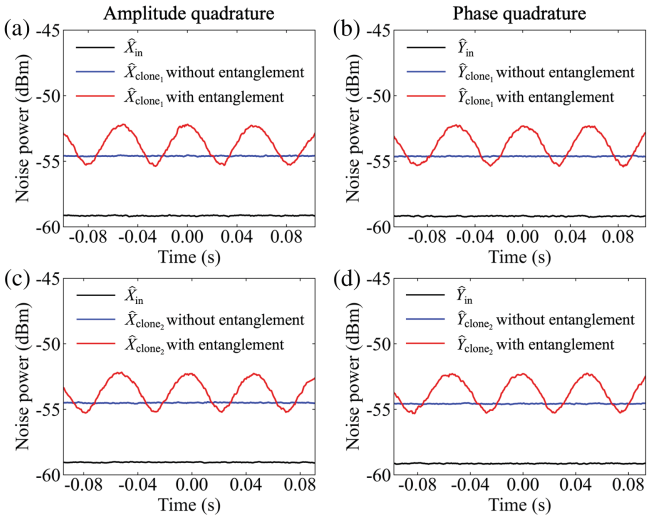

FIG. 3. The typical results of all-optical $1 \rightarrow 2$ CV quantum telecloning. (a)[(b)] The variances of amplitude quadrature (phase quadrature) of clone$_1$. (c)[(d)] The variances of amplitude quadrature (phase quadrature) of clone$_2$. The black solid traces represent the variances of amplitude quadrature (phase quadrature) of the input state. The blue solid traces represent the variances of amplitude quadrature (phase quadrature) of the corresponding classical limits. The red solid traces are noise power of the photocurrents output from BHD versus the scanning phase.

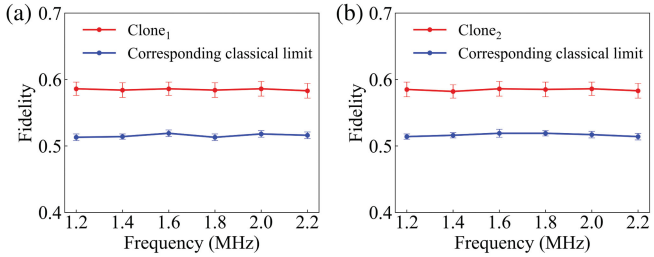

FIG. 4. The experimental fidelities versus the sideband frequency. The fidelities of all-optical $1 \rightarrow 2$ quantum telecloning [(a) clone$_1$ and (b) clone$_2$] and corresponding experimental classical limits are shown as the red traces and the blue traces, respectively. The error bars are obtained from the standard deviations of multiple repeated measurements.

quadrature $\hat{Y}_{\text{clone}_1}$ ($\hat{Y}_{\text{clone}_2}$) for the clone$_1$ (clone$_2$) measured by blocking the tripartite entanglement source, which correspond to the classical limits. It can be seen that the variances of $\hat{X}_{\text{clone}_1}$ and $\hat{Y}_{\text{clone}_1}$ ($\hat{X}_{\text{clone}_2}$ and $\hat{Y}_{\text{clone}_2}$) without entanglement for the clone$_1$ (clone$_2$) are 4.55 ± 0.06 and 4.56 ± 0.05 dB (4.55 ± 0.04 and 4.57 ± 0.08 dB), respectively, above the corresponding variances of input state $\hat{X}_{\text{in}}$ and $\hat{Y}_{\text{in}}$. This gives the fidelity of the classical limit of telecloning for the clone$_1$ (clone$_2$), i.e., $51.9\% \pm 0.5\%$ ($51.9\% \pm 0.6\%$). The corresponding theoretical classical limit is 52.6%. Such a difference is due to the extra noise introduced by PA based on FWM$_2$. The red solid traces shown in Figs. 3(a) and 3(b) [Figs. 3(c) and 3(d)] are the variances of amplitude quadrature $\hat{X}_{\text{clone}_1}$ ($\hat{X}_{\text{clone}_2}$) and phase quadrature $\hat{Y}_{\text{clone}_1}$ ($\hat{Y}_{\text{clone}_2}$) for the clone$_1$ (clone$_2$) with the assistance of the tripartite entanglement source, respectively. The relative phase between the beams $\hat{a}_2$ and $\hat{b}_1$ ($\hat{a}_3$ and $\hat{b}_1$) is scanned by a PZT. When the variances of amplitude and phase quadratures reach the minima of the red solid traces in Fig. 3, the relative phase between the beams $\hat{a}_2$ and $\hat{b}_1$ ($\hat{a}_3$ and $\hat{b}_1$) corresponds to $\hat{X}_{\hat{a}_2} - \hat{X}_{\hat{b}_1}$ and $\hat{Y}_{\hat{a}_2} + \hat{Y}_{\hat{b}_1}$ ($\hat{X}_{\hat{a}_3} - \hat{X}_{\hat{b}_1}$ and $\hat{Y}_{\hat{a}_3} + \hat{Y}_{\hat{b}_1}$). Therefore, we can regard the minima of the red solid traces in Figs. 3(a) and 3(b) [Figs. 3(c) and 3(d)] as the variances of $\hat{X}_{\text{clone}_1}$ and $\hat{Y}_{\text{clone}_1}$ ($\hat{X}_{\text{clone}_2}$ and $\hat{Y}_{\text{clone}_2}$), respectively. It can be seen from Figs. 3(a) and 3(b) that the variances of $\hat{X}_{\text{clone}_1}$ and $\hat{Y}_{\text{clone}_1}$ with entanglement are 3.83 ± 0.11 and 3.82 ± 0.10 dB, respectively, above the corresponding variances of input state $\hat{X}_{\text{in}}$ and $\hat{Y}_{\text{in}}$. Similarly, the variances of $\hat{X}_{\text{clone}_2}$ and $\hat{Y}_{\text{clone}_2}$ shown in Figs. 3(c) and 3(d) are 3.82 ± 0.10 and 3.84 ± 0.13 dB, respectively, above the corresponding variances of input state $\hat{X}_{\text{in}}$ and $\hat{Y}_{\text{in}}$. Based on Eq. (6), we can find that the fidelities of two clones in all-optical $1 \rightarrow 2$ quantum telecloning protocol are $58.6\% \pm 1.0\%$ and $58.6\% \pm 1.1\%$, respectively, exceeding the corresponding classical limits ($51.9\% \pm 0.5\%$ and $51.9\% \pm 0.6\%$). Therefore, we can claim that our all-optical $1 \rightarrow 2$ quantum telecloning scheme is successfully implemented.

In order to demonstrate the advantage of the all-optical $1 \rightarrow 2$ CV quantum telecloning scheme, which avoids optic-electro and electro-optic conversions, we verify that all-optical $1 \rightarrow 2$ quantum telecloning can be realized in the bandwidth range from 1.2 to 2.2 MHz. The corresponding experimental results are shown in Fig. 4. The red solid traces represent the fidelities of all-optical $1 \rightarrow 2$ quantum telecloning, and the blue solid traces represent the corresponding classical limits. It can be clearly seen from Fig. 4 that the fidelities of all-optical $1 \rightarrow 2$ quantum telecloning protocol exceed the corresponding classical limits, which proves that we can implement the all-optical $1 \rightarrow 2$ quantum telecloning scheme successfully within the bandwidth range from 1.2 to 2.2 MHz. In our scheme, the bandwidth is mainly limited by the squeezing bandwidth of FWM process [40]. In the future, to improve the bandwidth of all-optical quantum telecloning, other broadband entanglement can be utilized. Recently, based on the periodically poled $LiNbO_3$ waveguide, the THz sideband CV quantum squeezing has been successfully demonstrated [41–43]. Based on such a scheme, an ultrabroadband all-optical quantum telecloning is promising to be constructed in the future.

In conclusion, we have experimentally implemented an all-optical CV quantum telecloning protocol. Our study exhibits coherent state $1 \rightarrow 2$ quantum telecloning with fidelities of $58.6\% \pm 1.0\%$ and $58.6\% \pm 1.1\%$ for the two

clones, surpassing the corresponding classical limit. Moreover, we show that all-optical $1 \rightarrow 2$ quantum telecloning can be implemented with a bandwidth ranging from 1.2 to 2.2 MHz. Our work has established a concise platform for constructing quantum telecloning. More importantly, our scheme can be easily generalized to all-optical $1 \rightarrow M$ quantum telecloning by exploiting $(M+1)$-mode entanglement source based on one pair of EPR and M BSs. Our scheme provides a new path to construct high-bandwidth quantum communication networks.

This work was funded by the National Natural Science Foundation of China (No. 12225404, No. 11874155, No. 91436211, No. 11374104, and No. 12174110); Innovation Program of Shanghai Municipal Education Commission (Grant No. 2021-01-07-00-08-E00100); Program of Shanghai Academic Research Leader (No. 22XD1400700); Basic Research Project of Shanghai Science and Technology Commission (No. 20JC1416100); Natural Science Foundation of Shanghai (No. 17ZR1442900); Minhang Leading Talents (No. 201971); Shanghai Sailing Program (No. 21YF1410800); Natural Science Foundation of Chongqing (No. CSTB2022NSCQ-MSX0893); Shanghai Municipal Science and Technology Major Project (No. 2019SHZDZX01); and the 111 project (B12024).

*These authors contributed equally to this letter.
†Corresponding author: ssliu@lps.ecnu.edu.cn
‡Corresponding author: jtjing@phy.ecnu.edu.cn

[1] W. K. Wootters and W. H. Zurek, A single quantum cannot be cloned, Nature (London) **299**, 802 (1982).
[2] D. Dieks, Communication by EPR devices, Phys. Lett. **92A**, 271 (1982).
[3] V. Scarani, S. Iblisdir, N. Gisin, and A. Acín, Quantum cloning, Rev. Mod. Phys. **77**, 1225 (2005).
[4] W. T. M. Irvine, A. Lamas Linares, M. J. A. de Dood, and D. Bouwmeester, Optimal quantum cloning on a beam splitter, Phys. Rev. Lett. **92**, 047902 (2004).
[5] A. Lamas-Linares, C. Simon, J. C. Howell, and D. Bouwmeester, Experimental quantum cloning of single photons, Science **296**, 712 (2002).
[6] N. J. Cerf, A. Ipe, and X. Rottenberg, Cloning of continuous quantum variables, Phys. Rev. Lett. **85**, 1754 (2000).
[7] N. J. Cerf and S. Iblisdir, Optimal N-to-M cloning of conjugate quantum variables, Phys. Rev. A **62**, 040301(R) (2000).
[8] J. Fiurášek, Optical implementation of continuous-variable quantum cloning machines, Phys. Rev. Lett. **86**, 4942 (2001).
[9] S. L. Braunstein, N. J. Cerf, S. Iblisdir, P. van Loock, and S. Massar, Optimal cloning of coherent states with a linear amplifier and beam splitters, Phys. Rev. Lett. **86**, 4938 (2001).
[10] S. Liu, Y. Lou, Y. Chen, and J. Jing, All-optical optimal N-to-M quantum cloning of coherent states, Phys. Rev. Lett. **126**, 060503 (2021).
[11] U. L. Andersen, V. Josse, and G. Leuchs, Unconditional quantum cloning of coherent states with linear optics, Phys. Rev. Lett. **94**, 240503 (2005).
[12] M. Sabuncu, U. L. Andersen, and G. Leuchs, Experimental demonstration of continuous variable cloning with phase-conjugate inputs, Phys. Rev. Lett. **98**, 170503 (2007).
[13] J. Y. Haw, J. Zhao, J. Dias, S. M. Assad, M. Bradshaw, R. Blandino, T. Symul, T. C. Ralph, and P. K. Lam, Surpassing the no-cloning limit with a heralded hybrid linear amplifier for coherent states, Nat. Commun. **7**, 13222 (2016).
[14] A. Furusawa, J. L. Sørensen, S. L. Braunstein, C. A. Fuchs, H. J. Kimble, and E. S. Polzik, Unconditional quantum teleportation, Science **282**, 706 (1998).
[15] S. L. Braunstein and H. J. Kimble, Teleportation of continuous quantum variables, Phys. Rev. Lett. **80**, 869 (1998).
[16] M. Huo, J. Qin, J. Cheng, Z. Yan, Z. Qin, X. Su, X. Jia, C. Xie, and K. Peng, Deterministic quantum teleportation through fiber channels, Sci. Adv. **4**, eaas9401 (2018).
[17] N. Lee, H. Benichi, Y. Takeno, S. Takeda, J. Webb, E. Huntington, and A. Furusawa, Teleportation of nonclassical wave packets of light, Science **332**, 330 (2011).
[18] T. C. Ralph, All-optical quantum teleportation, Opt. Lett. **24**, 348 (1999).
[19] S. Liu, Y. Lou, and J. Jing, Orbital angular momentum multiplexed deterministic all-optical quantum teleportation, Nat. Commun. **11**, 3875 (2020).
[20] S. Liu, Y. Lou, Y. Chen, and J. Jing, All-optical entanglement swapping, Phys. Rev. Lett. **128**, 060503 (2022).
[21] S. Shen, C. Yuan, Z. Zhang, H. Yu, R. Zhang, C. Yang, H. Li, Z. Wang, Y. Wang, G. Deng, H. Song, L. You, Y. Fan, G. Guo, and Q. Zhou, Hertz-rate metropolitan quantum teleportation, Light Sci. Appl. **12**, 115 (2023).
[22] Z. Yan and X. Jia, Teleportation goes to Hertz rate, Light Sci. Appl. **12**, 167 (2023).
[23] M. Murao, D. Jonathan, M. B. Plenio, and V. Vedral, Quantum telecloning and multiparticle entanglement, Phys. Rev. A **59**, 156 (1999).
[24] P. van Loock and S. L. Braunstein, Telecloning of continuous quantum variables, Phys. Rev. Lett. **87**, 247901 (2001).
[25] S. Koike, H. Takahashi, H. Yonezawa, N. Takei, S. L. Braunstein, T. Aoki, and A. Furusawa, Demonstration of quantum telecloning of optical coherent states, Phys. Rev. Lett. **96**, 060504 (2006).
[26] Q. Wang, W. Li, Y. Wu, W. Yao, F. Li, L. Tian, Y. Wang, and Y. Zheng, Demonstration of $1 \rightarrow 3$ continuous-variable quantum telecloning, Phys. Rev. A **104**, 032419 (2021).
[27] S. Takeda and A. Furusawa, Toward large-scale fault-tolerant universal photonic quantum computing, APL Photonics **4**, 060902 (2019).
[28] C. F. McCormick, V. Boyer, E. Arimondo, and P. D. Lett, Strong relative intensity squeezing by four-wave mixing in rubidium vapor, Opt. Lett. **32**, 178 (2007).
[29] V. Boyer, A. M. Marino, R. C. Pooser, and P. D. Lett, Entangled images from four-wave mixing, Science **321**, 544 (2008).
[30] A. M. Marino, R. C. Pooser, V. Boyer, and P. D. Lett, Tunable delay of Einstein–Podolsky–Rosen entanglement, Nature (London) **457**, 859 (2009).
[31] R. C. Pooser, N. Savino, E. Batson, J. L. Beckey, J. Garcia, and B. J. Lawrie, Truncated nonlinear interferometry for

quantum-enhanced atomic force microscopy, Phys. Rev. Lett. **124**, 230504 (2020).

[32] S. Liu, Y. Lou, and J. Jing, Interference-induced quantum squeezing enhancement in a two-beam phase-sensitive amplifier, Phys. Rev. Lett. **123**, 113602 (2019).

[33] Y. Chen, Q. Zhu, X. Wang, Y. Lou, S. Liu, and J. Jing, Deterministic all-optical quantum state sharing, Adv. Photonics **5**, 026006 (2023).

[34] A. Einstein, B. Podolsky, and N. Rosen, Can quantum-mechanical description of physical reality be considered complete?, Phys. Rev. **47**, 777 (1935).

[35] X. Zuo, Z. Yan, Y. Feng, J. Ma, X. Jia, C. Xie, and K. Peng, Quantum interferometer combining squeezing and parametric amplification, Phys. Rev. Lett. **124**, 173602 (2020).

[36] X. Guo, C. R. Breum, J. Borregaard, S. Izumi, M. V. Larsen, T. Gehring, M. Christandl, J. S. Neergaard-Nielsen, and U. L. Andersen, Distributed quantum sensing in a continuous-variable entangled network, Nat. Phys. **16**, 281 (2020).

[37] J. Jing, J. Zhang, Y. Yan, F. Zhao, C. Xie, and K. Peng, Experimental demonstration of tripartite entanglement and controlled dense coding for continuous variables, Phys. Rev. Lett. **90**, 167903 (2003).

[38] F. A. S. Barbosa, A. S. Coelho, A. J. de Faria, K. N. Cassemiro, A. S. Villar, P. Nussenzveig, and M. Martinelli, Robustness of bipartite Gaussian entangled beams propagating in lossy channels, Nat. Photonics **4**, 858 (2010).

[39] S. L. Braunstein, C. A. Fuchs, H. J. Kimble, and P. van Loock, Quantum versus classical domains for teleportation with continuous variables, Phys. Rev. A **64**, 022321 (2001).

[40] L. E. E. De Araujo, Z. Zhou, M. Dimario, B. E. Anderson, J. Zhao, K. M. Jones, and P. D. Lett, Properties of two-mode quadrature squeezing from four-wave mixing in rubidium vapor, arXiv:2310.11900.

[41] R. Nehra, R. Sekine, L. Ledezma, Q. Guo, R. M. Gray, A. Roy, and A. Marandi, Few-cycle vacuum squeezing in nanophotonics, Science **377**, 1333 (2022).

[42] T. Kashiwazaki, T. Yamashima, N. Takanashi, A. Inoue, T. Umeki, and A. Furusawa, Fabrication of low-loss quasi-single-mode PPLN waveguide and its application to a modularized broadband high-level squeezer, Appl. Phys. Lett. **119**, 251104 (2021).

[43] T. Kashiwazaki, N. Takanashi, T. Yamashima, T. Kazama, K. Enbutsu, R. Kasahara, T. Umeki, and A. Furusawa, Continuous-wave 6-dB-squeezed light with 2.5-THz-bandwidth from single-mode PPLN waveguide, APL Photonics **5**, 036104 (2020).